Electronic Supplementary Material (ESI) for Physical Chemistry Chemical Physics.

Supporting information for

Temperature- and pressure-dependent studies of niccolite-type formate frameworks of $[NH_3(CH_2)_4NH_3][M_2(HCOO)_6]$ (M=Zn, Co, Fe)

Mirosław Mączka,[a] Maciej Ptak,[a] Sebastian Pawlus,[b] Waldeci Paraguassu,[c] Adam Sieradzki,[d] Sergejus Balciunas,[e] Mantas Simenas,[e] and Juras Banys[e]*

[a]*Institute of Low Temperature and Structure Research, Polish Academy of Sciences, Box 1410, 50-950 Wrocław 2, Poland*

[b]*Institute of Physics, University of Silesia, ul. Uniwersytecka 4, 40-007 Katowice, Poland*

[c]*Faculdade de Física, Universidade Federal do Pará, 66075-110, Belém, PA, Brazil*

[d]*Department of Experimental Physics, Wrocław University of Technology, Wybrzeże Wyspiańskiego 27, 50-370, Wrocław, Poland*

[e]*Faculty of Physics, Vilnius University, Sauletekio av. 9, LT-10222 Vilnius, Lithuania*

e-mail: m.maczka@int.pan.wroc.pl

Table S1. IR wavenumbers (in cm^{-1}) of bnZn, bnCo and bnFe and proposed assignments.[a]

bnZn		bnCo		bnFe		
294 K	5 K	294 K	5 K	294 K	5 K	assignment
3167sh	3197w, 3171vw	3196sh	3214sh, 3192w	3173sh	3188w	$\nu(NH_3)$
	3153w	3166sh				
	3125w, 3095m		3130sh, 3103m		3130w, 3103m	$\nu(NH_3)$
3050m	3056m, 3031w	3054m	3059w	3053m	3061m	$\nu(NH_3)$
3031vw	3034vw		3033w, 3026w		3032sh	$\nu(NH_3)$
3004w	3003m	3003w	3005m, 2991m	3003w	3001s, 2982sh	$\nu_{as}(CH_2)$
2944m	2948sh, 2939m	2940m	2948m, 2939m	2941m	2946sh, 2929m	$\nu_{as}(CH_2)$
	2930sh		2928m			
2904w	2904w		2901w	2910w	2902w	$\nu_s(CH_2)$
2878w	2886w, 2868w	2872vw	2876m	2871sh	2870w	$\nu_s(CH_2)$
2845m	2855m, 2843m	2850m	2850m, 2838sh	2843s	2843s	$\nu_1(HCOO^-)$
2803sh	2813m	2804w	2814w	2804sh	2806w	overtones
2790sh	2797m	2790sh	2798w	2784sh	2796w	overtones
2103w,b	2152w, 2135w	2102w,b	2142w	2098w	2130w	$\delta_{as}(NH_3)+ \tau(NH_3)$
	2122w					
	1655vw	1653vw	1654w	1649w	1653w	$\delta_{as}(NH_3)$
1637sh	1644sh, 1432w	1632sh,	1642w, 1434w	1632sh	1644w	$\delta_{as}(NH_3)$
1592s	1602s, 1584s	1592s	1597s, 1585s	1588s	1590s	$\nu_4(HCOO^-)$
1520w,b	1536w, 1527w	1521w	1529w, 1535w	1522w	1531w	$\delta_s(NH_3)$
1456w, 1449w	1458m, 1455sh 1447w	1456w, 1449w	1457w, 1450w	1455w, 1450w	1456w, 1449w	$\delta(CH_2)$

1373s	1381s, 1374s	1372s	1382sh, 1377s 1373s	1373s	1374s	$\nu_5(HCOO^-)$
1356sh 1345s	1360w, 1352s 1343s	1356s 1348s	1362sh, 1359s 1354s, 1351sh, 1345s	1356sh 1347s	1357s, 1352s 1346s	$\nu_2(HCOO^-)$
1316w	1318w, 1315w		1320vw		1319w	$\omega(CH_2)$
1304sh	1302w	1294vw	1292w	1295vw	1293w	$\omega(CH_2)$
1270w	1270w	1270w	1271w	1269w	1270w	$\tau(CH_2)$
1262w	1260vw	1263w	1263w	1262w	1263w	$\tau(CH_2)$
1189vw	1193w	1189vw	1193vw	1184vw	1191w	$\tau(CH_2)$
1170w	1174w	1172w	1174w	1171w	1174w	$\rho(NH_3)$
1110w	1112w	1111w	1113w, 1111sh	1111vw	1128w, 1113w	$\rho(NH_3)$
1099w	1101w	1098w	1100w	1101w	1101w	$\rho(NH_3)$
1077w	1088w		1088w		1088vw, 1081vw	$\nu(CC)$
1070w	1080w, 1077w	1070w	1069w	1072w		$\nu_6(HCOO^-)$
1056w	1062w	1056w		1056w	1060w	$\nu(CC)$
1032w	1039w, 1035w	1033w	1037w, 1034w	1031w	1035w	$\nu(CC)$
1024w	1027w, 1024w	1024w	1027w, 1024w	1023w	1027w	$\nu(CC)$
1000w	1007vw, 1003w	1001w	1004w	1001w	1004w	$\nu(CC) + \nu(CN)$
984w	992w, 988w	984w	991w	982w	991w	$\nu(CC) + \nu(CN)$
917vw	923vw, 919w	917vw	920w	917vw	920w	$\nu(CN)$
910w	912w	910vw		908w	913w	overtone
889w	894w, 885w	888w	894w, 887sh	886w	892w, 887sh	$\rho(NH_3)$
872vw	873w	872w	874w	872vw	873w	$\nu(CN)$
844vw	847w	844vw	846w	843vw	846w	overtone
799s	817w, 809w 802s, 795sh	803s	816sh, 811sh 805s	813sh, 798s	819sh, 814sh 801s	$\nu_3(HCOO^-)$
750vw	752w	752vw	752w	751vw	752w	$\rho(CH_2)$

742w	745w	743w	745w	741w	744w	$\rho(CH_2)$
524w	527w	524w	527w	522w	527w	δ(CCC)
495w	502w, 497w	496vw	496vw	496w	497w	δ(CCC)
~493w,b	518w, 515w	~490w,b	516sh, 511w		~503w,b	$\tau(NH_3)$
450w	452w	450w	452w	448w	451w	δ(CCN)
422w	428m	423w	427m, 424sh	420w	435sh, 425w	δ(CCN)
			369sh	368m	376m	$T'(HCOO^-) + T'(M^{2+})$
304m	320m	321s	341s	313s	329s	$T'(HCOO^-) + T'(M^{2+})$
	295w, 285w		322sh, 311w		304w, 285w	$T'(HCOO^-) + T'(M^{2+})$
246m	262m, 256m	268m	286w, 278m	259m	268m	$T'(HCOO^-) + T'(M^{2+})$
	250w, 242m		261w			
204s	230vw, 212m	221sh	234w,			$T'(HCOO^-) + L(HCOO^-)$
	204m					
177s	192m, 182s	202s	215sh, 210w,	193s	201s, 189s	$T'(HCOO^-) + L(HCOO^-)$
	177s		205sh, 193sh			
	159vw, 152vw	160vw,b	177vw, 170vw		157w, 148w	$L(bnH_2^{2+}) + T'(bnH_2^{2+})$
	148vw, 140vw		160w, 155w			
	132vw, 126vw		138vw			
100vw	105w, 99w, 88w	106w	109m, 101vw	100vw	101w	$L(bnH_2^{2+}) + T'(bnH_2^{2+})$
			92w			

[a]Key: s, strong; m, medium; w, weak; vw, very weak; sh, shoulder; b, broad; Internal vibrations of $HCOO^-$ ions are classified as C-H stretching (ν_1), symmetric C-O stretching (ν_2), antisymmetric C-O stretching (ν_4), symmetric O-C-O bending (ν_3), C-H in-plane bending (ν_5) and C-H out-of-plane bending (ν_6) modes. Internal vibrations of bnH_2^{2+} cation are subdivided into symmetric stretching ($\nu_s(CH_2)$), antisymmetric stretching (($\nu_{as}(CH_2)$), scissoring ($\delta(CH_2)$), rocking ($\rho(CH_2)$), wagging ($\omega(CH_2)$) and torsion or twisting ($\tau(CH_2)$) modes of the CH_2 groups as well as symmetric stretching (ν_s), antisymmetric stretching (ν_{as}), bending (δ), rocking (ρ) and torsion (τ) modes of the NH_3 groups. The remaining vibrations correspond to CC and CN stretching as well as CCN in-plane bending and out-of-plane bending modes.

Table S2. Raman wavenumbers (in cm^{-1}) of bnZn, bnCo and bnFe and proposed assignments.[a]

bnZn		bnCo		bnFe	
294 K	80 K	294 K	80 K	294 K	assignment
3011m	3012m	3009m	3010m	3007m	$\nu_{as}(CH_2)$
2972s	2977sh, 2971s	2971s	2976sh, 2971s	2972s	$\nu_{as}(CH_2)$
2942s	2949s, 2942s	2953sh, 2944s	2949s, 2941s	2940s	$\nu_{as}(CH_2)$
2896w	2906w, 2901w	2897w	2906sh, 2900w	2894w	$\nu_{s}(CH_2)$
	2892w				
2870sh	2874m	2871sh	2876m	2871sh	$\nu_{s}(CH_2)$
2854s	2855s, 2850s	2854s	2856s, 2852s	2850s	$\nu_1(HCOO^-)$
1645vw	1655vw		1650w		$\delta_{as}(NH_3)$
1632vw	1641vw	1634w	1642w	1637w	$\delta_{as}(NH_3)$
		1563w	1570w	1576w	$\nu_4(HCOO^-)$
1456w, 1440w	1458w, 1444w	1458vw, 1441w	1459w, 1445w	1458w, 1440w	$\delta(CH_2)$
1398sh	1400vw	1399vw	1400w		overtone
1374s	1375s, 1369sh	1371s	1372s, 1363w	1374s	$\nu_5(HCOO^-)$
1354m	1362m, 1357sh	1353m	1352m, 1346w	1360m	$\nu_2(HCOO^-)$
	1352m, 1346w				
1325w	1323w	1325w	1323w	1326w	$\omega(CH_2)$
1292w	1291w	1293vw	1292vw	1293w	$\omega(CH_2)$
1085w	1087w	1085vw	1088w	1087vw	$\nu(CC)$
1070w	1074w, 1067w	1069w	1072w	1068w	$\nu_6(HCOO^-)$
1050w	1058w	1057vw	1059w		$\nu(CC)$
1032w	1037w	1032w	1037w	1030w	$\nu(CC)$
1000w	1004w	1001vw		1000w	$\nu(CC) + \nu(CN)$
916w	923w	919w	922w	940w, 916w	$\nu(CN)$

887vw	892w	889vw	893w	887vw	$\rho(NH_3)$
874w	874w	874w	875vw	875w	ν(CN)
843vw	845w			854w	overtone
811m, 798m	815m, 801w	804sh, 798m	811m, 801m	810w, 800s	$\nu_3(HCOO^-)$
790sh	793w	793sh	796sh		
751vw	751w			751w	$\rho(CH_2)$
522w	526w			522w	δ(CCC)
513w	511w			512w	δ(CCC)
312vw	318w		303w	312w	$T'(HCOO^-) + T'(M^{2+})$
260vw	281w, 274w	266sh	283w		$T'(HCOO^-) + T'(M^{2+})$
210sh	236w, 221w	242m	255m, 240m		$T'(HCOO^-) + T'(M^{2+})$
189m	203m, 192m	198m	214m, 199m	189s	$L(HCOO^-)$
	181m				
144m	165w, 147m	152m	178m, 151m	143sh	$L(HCOO^-)$
		115m	126m		
108w	122w, 102m	92m	103w, 98m		$L(bnH_2^{2+}) + T'(bnH_2^{2+})$
			75w, 68w		$L(bnH_2^{2+}) + T'(bnH_2^{2+})$

[a]Key: s, strong; m, medium; w, weak; vw, very weak; sh, shoulder; b, broad.

Table S3. The correlation diagram showing the correspondence between the optical modes of $HCOO^-$ in the $P\bar{3}1c$ and $R\bar{3}c$ structures of bnZn or bnCo as well as the $P\bar{3}1c$ and Cc structures of bnMn (the data for the low-temperature structures are given in parentheses). Raman- and IR-active modes are denoted by blue and red color and the modes acive both in Raman and IR spectra are denoted by green color.

bnZn and bnCo				
ion	vibration	Free ion symmetry	Site symmetry	Factor group symmetry
HCOO-		**C_{2v}**	**C_1 (C_1)**	**D_{3d} (D_{3d})**
	ν_1, ν_2 or ν_3	A_1	A (12A)	$A_{1g}+A_{2g}+2E_g+A_{1u}+A_{2u}+2E_u$ ($12A_{1g}+12A_{2g}+24E_g+12A_{1u}+12A_{2u}+24E_u$)
	ν_4, ν_5 or ν_6	B_1	A (12A)	$A_{1g}+A_{2g}+2E_g+A_{1u}+A_{2u}+2E_u$ ($12A_{1g}+12A_{2g}+24E_g+12A_{1u}+12A_{2u}+24E_u$)
	T’	$A_1 + B_1 + B_2$	3A (36A)	$3A_{1g}+3A_{2g}+6E_g+3A_{1u}+3A_{2u}+6E_u$ ($36A_{1g}+36A_{2g}+72E_g+36A_{1u}+36A_{2u}+72E_u$)
	L	$A_2 + B_1 + B_2$	3A (36A)	$3A_{1g}+3A_{2g}+6E_g+3A_{1u}+3A_{2u}+6E_u$ ($36A_{1g}+36A_{2g}+72E_g+36A_{1u}+36A_{2u}+72E_u$)
bnMn				
ion	vibration	Free ion symmetry	Site symmetry	Factor group symmetry
HCOO-		**C_{2v}**	**C_1 (C_1)**	**D_{3d} (C_s)**
	ν_1, ν_2 or ν_3	A_1	A (6A)	$A_{1g}+A_{2g}+2E_g+A_{1u}+A_{2u}+2E_u$ (6A’+6A”)
	ν_4, ν_5 or ν_6	B_1	A (6A)	$A_{1g}+A_{2g}+2E_g+A_{1u}+A_{2u}+2E_u$ (6A’+6A”)
	T’	$A_1 + B_1 + B_2$	3A (18A)	$3A_{1g}+3A_{2g}+6E_g+3A_{1u}+3A_{2u}+6E_u$ (18A’+18A”)
	L	$A_2 + B_1 + B_2$	3A (18A)	$3A_{1g}+3A_{2g}+6E_g+3A_{1u}+3A_{2u}+6E_u$ (18A’+18A”)

Table S4. Wavenumber intercepts at zero pressure (ω_0) and pressure coefficients ($\alpha=d\omega/dP$), obtained from fitting of the experimental data by linear functions, for the ambient and high-pressure phases of bnZn.

ambient pressure phase		high-pressure phase		assignment
ω_0 (cm^{-1})	α ($cm^{-1}GPa^{-1}$)	ω_0 (cm^{-1})	α ($cm^{-1}GPa^{-1}$)	
1086.7	2.85			ν(CC)
1071.2	2.66	1066.3	5.72	$\nu_6(HCOO^-)$
1035.8	2.98			ν(CC)
1002.1	2.61	1007.2	2.28	ν(CC) + ν(CN)
917.4	1.02	901.2	5.34	ν(CN)
891.7	3.58			$\rho(NH_3)$
874.5	4.09	875.8	3.69	ν(CN)
811.9	3.98	800.8	4.00	$\nu_3(HCOO^-)$
799.5	2.74	812.3	-0.35	$\nu_3(HCOO^-)$
789.3	2.55	797.6	0.98	$\nu_3(HCOO^-)$
523.2	3.16			δ(CCC)
514.3	2.95	513.9	2.99	δ(CCC)
		273.1	11.13	T'($HCOO^-$) + T'(Zn^{2+})
		221.0	12.85	T'($HCOO^-$) + T'(Zn^{2+})
206.0	5.27	218.7	5.98	T'($HCOO^-$) + T'(Zn^{2+})
189.9	4.74	199.4	5.46	L($HCOO^-$)
		197.9	1.79	L($HCOO^-$)
		166.0	3.81	L($HCOO^-$)
144.2	2.61	156.9	3.37	L($HCOO^-$)

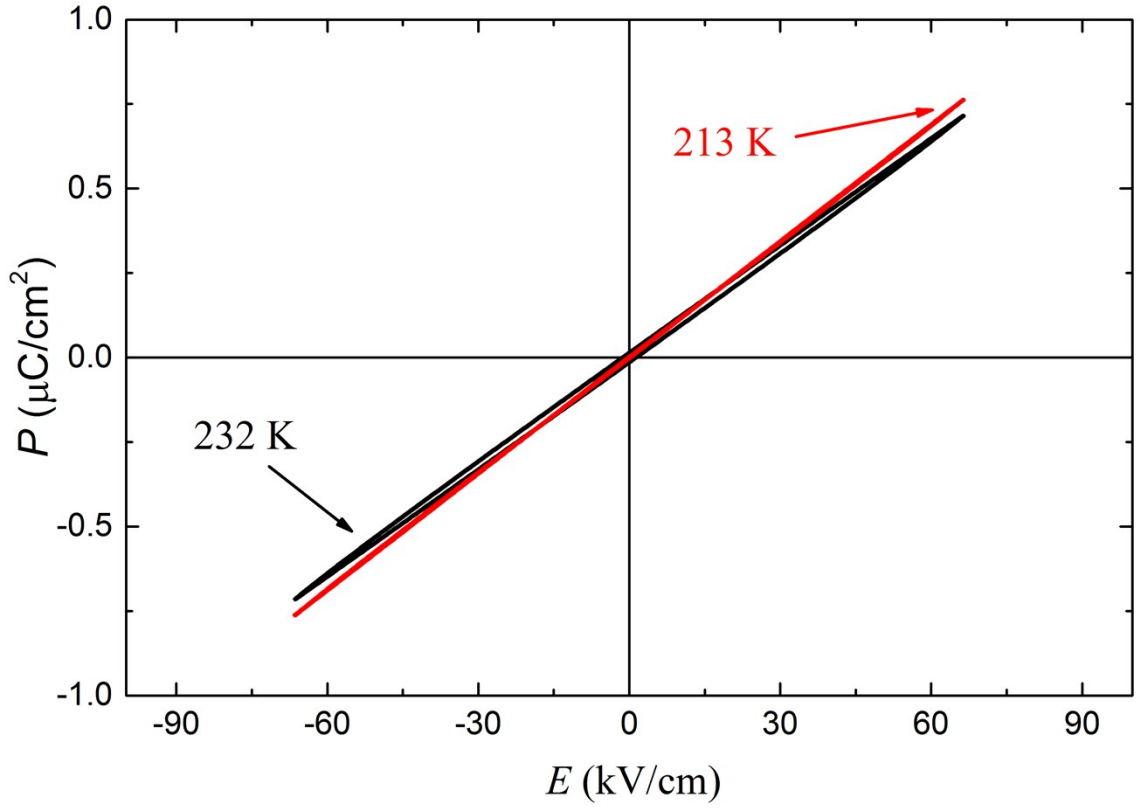

.

Figure S1. Electric field dependence of the electric polarization of bnZn measured at 232 K and 213 K. Measurement performed along the *c*-crystal axis.

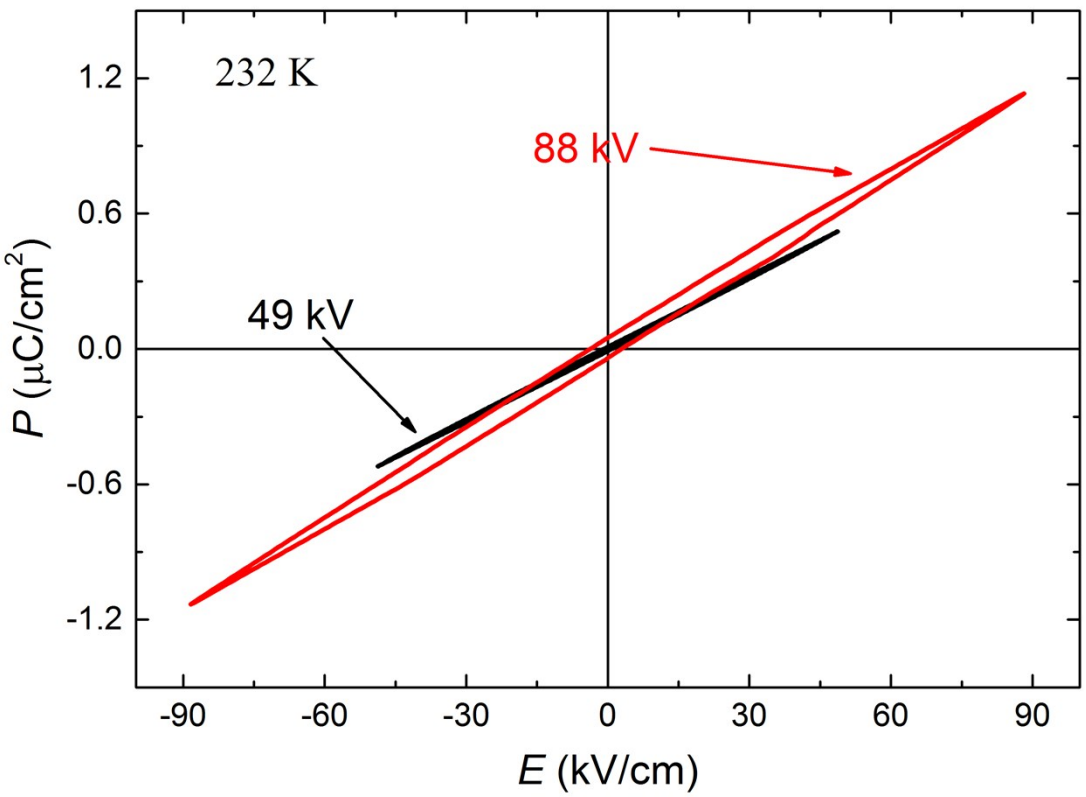

Figure S2. Electric field dependence of the electric polarization of bnZn obtained at 232 K for two different measuring voltages. Measurement performed along the *c*-crystal axis.

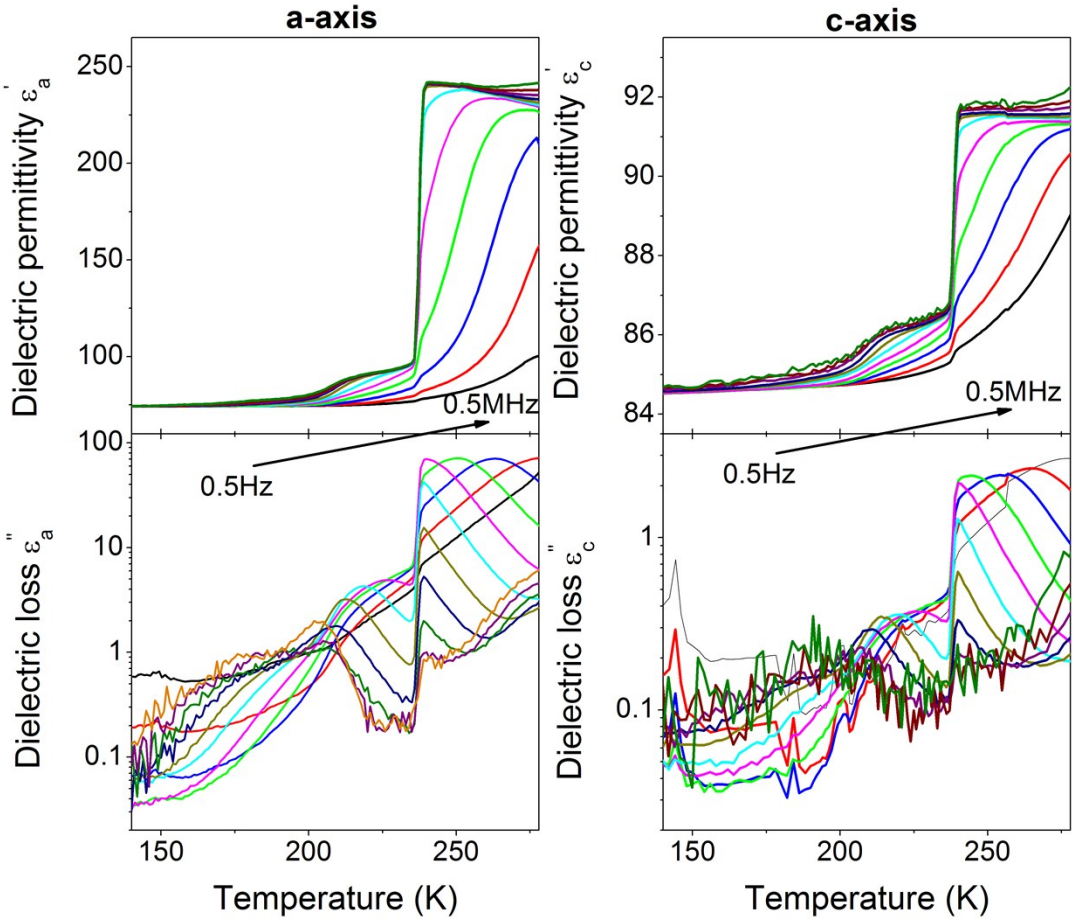

Figure S3. The temperature-dependent traces of the complex dielectric permittivity for two different crystallographic orientations along the *a*- and *c*-axis.

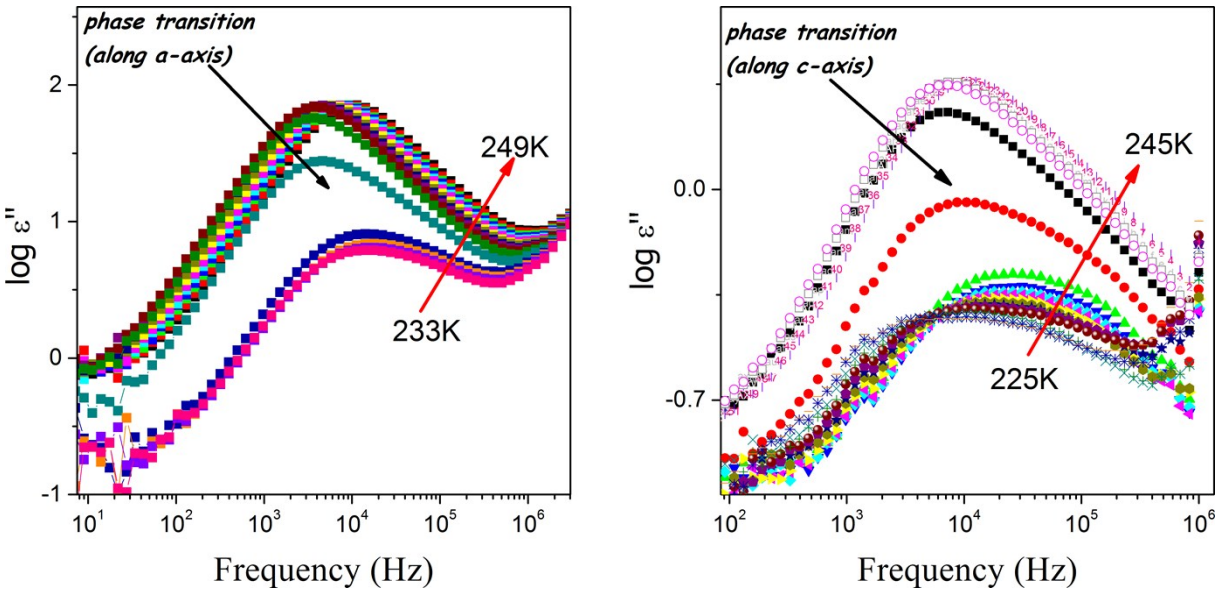

Figure S4. Frequency dependence of the complex dielectric permittivity for the investigated sample in two crystallographic directions.

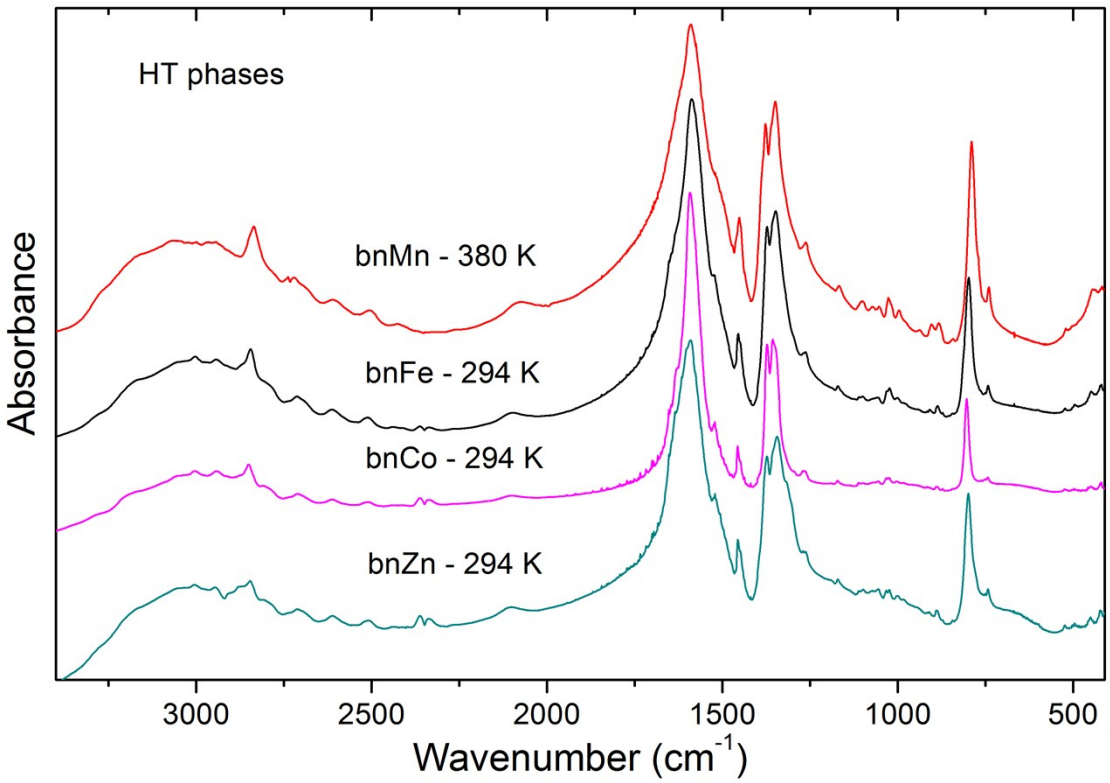

Figure S5. Room-temperature mid-IR spectra of the studied compounds. IR spectrum of the HT phase of bnMn is also shown. Similarity of the spectra confirms that the HT phases of all compounds are isostructural.

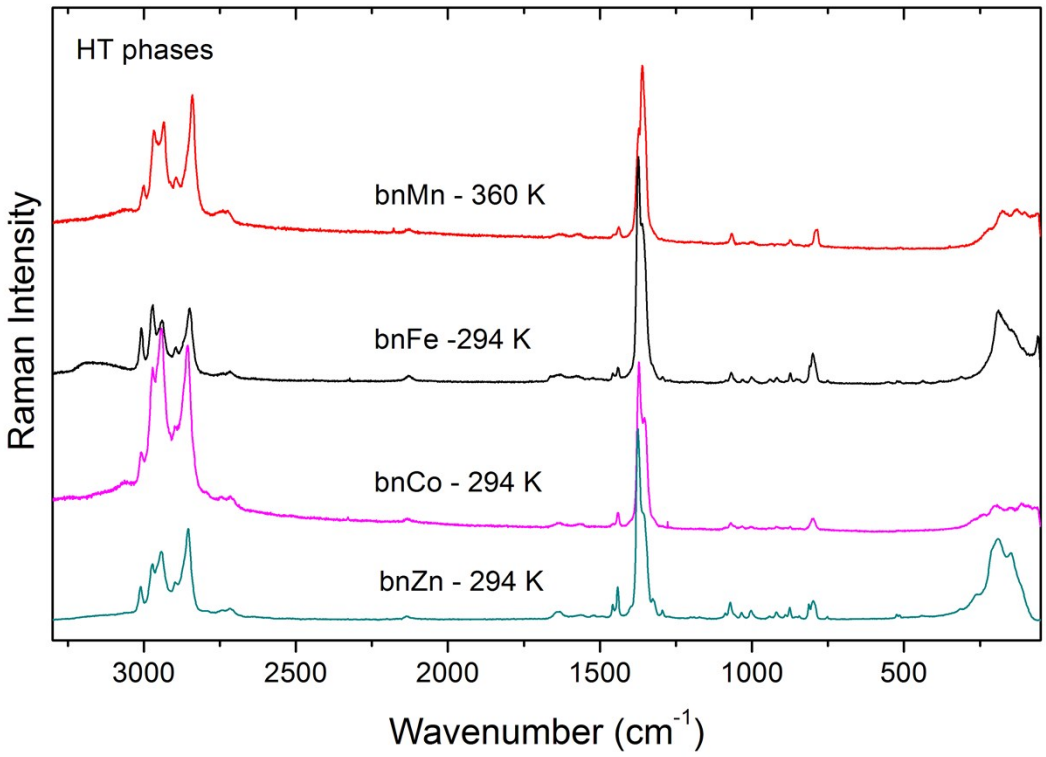

Figure S6. Room-temperature Raman spectra of the studied compounds. Raman spectrum of the HT phase of bnMn is also shown for the comparison sake.

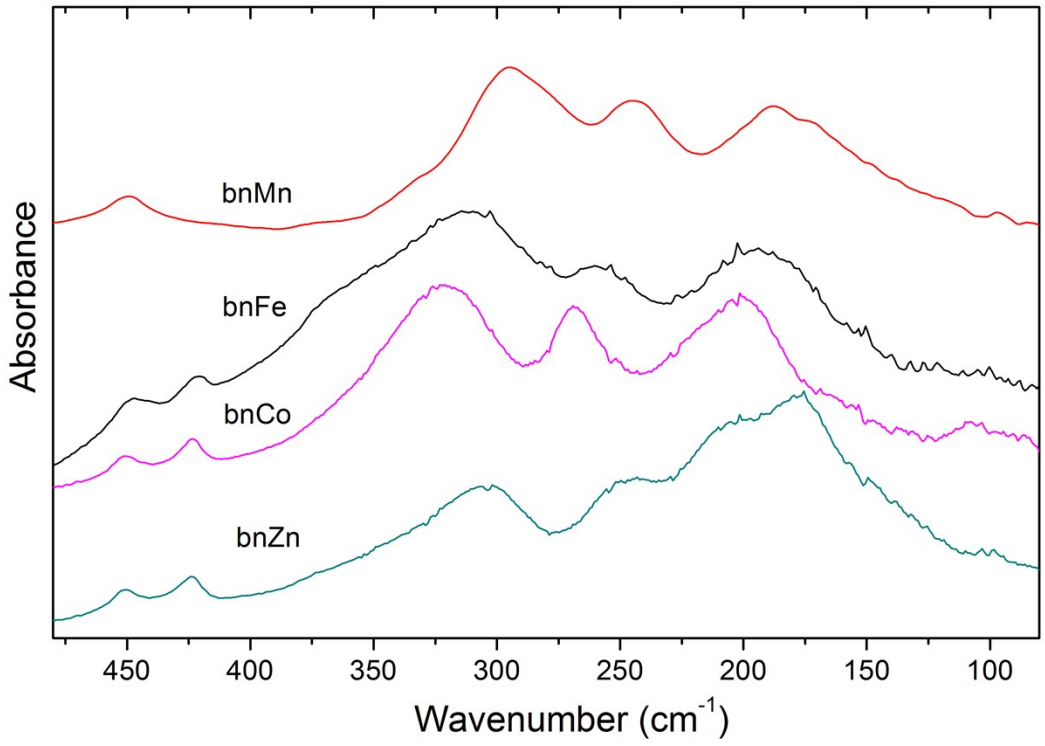

Figure S7. Room-temperature far-IR spectra of the studied compounds.

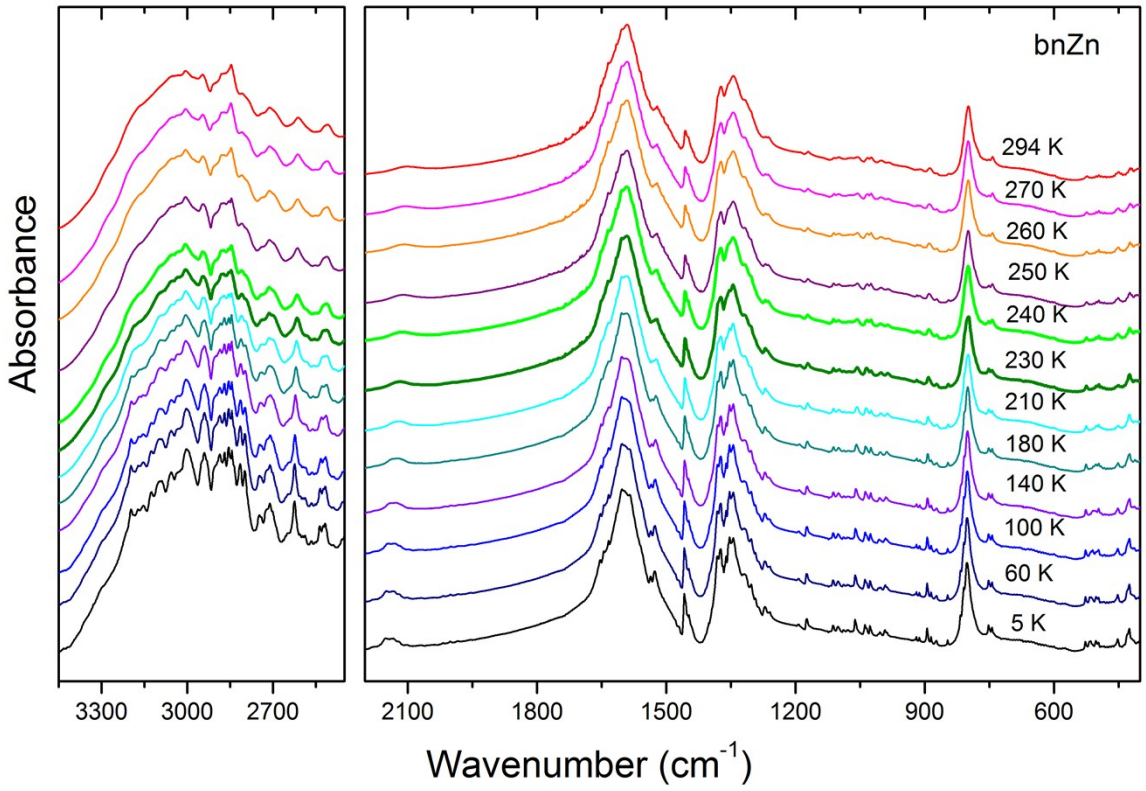

Figure S8. mid-IR spectra of bnZn recorded at various temperatures.

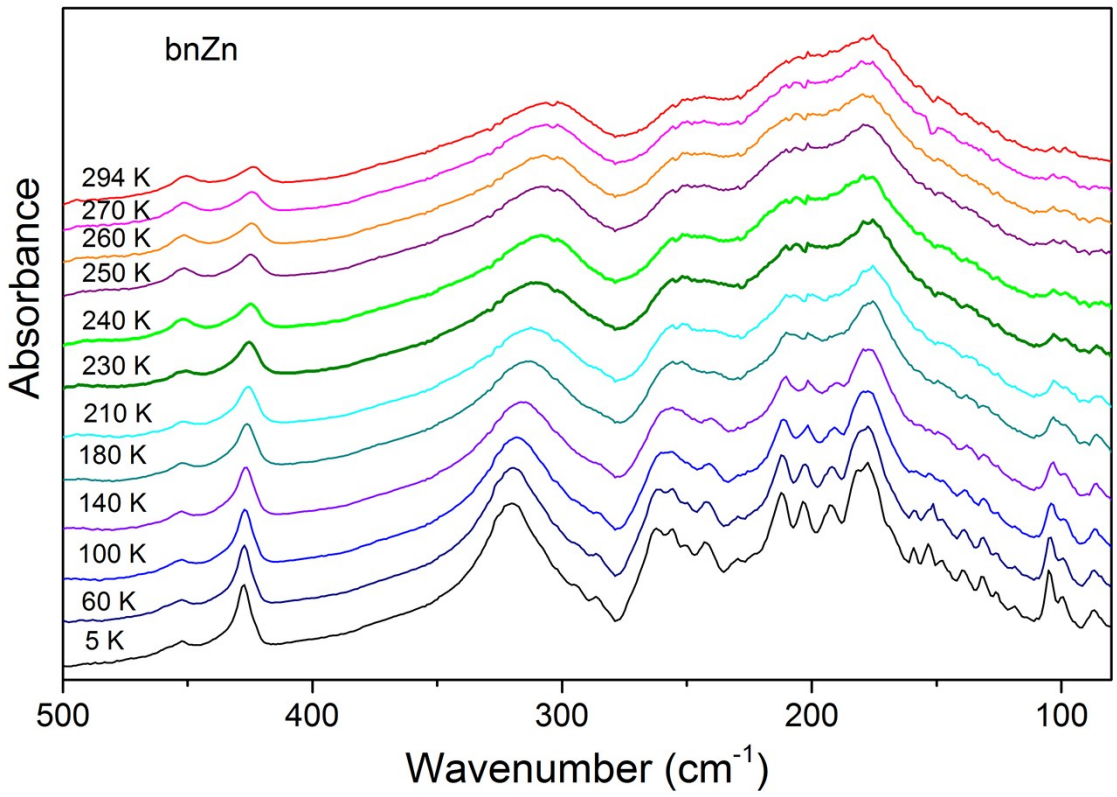

Figure S9. far-IR spectra of bnZn recorded at various temperatures.

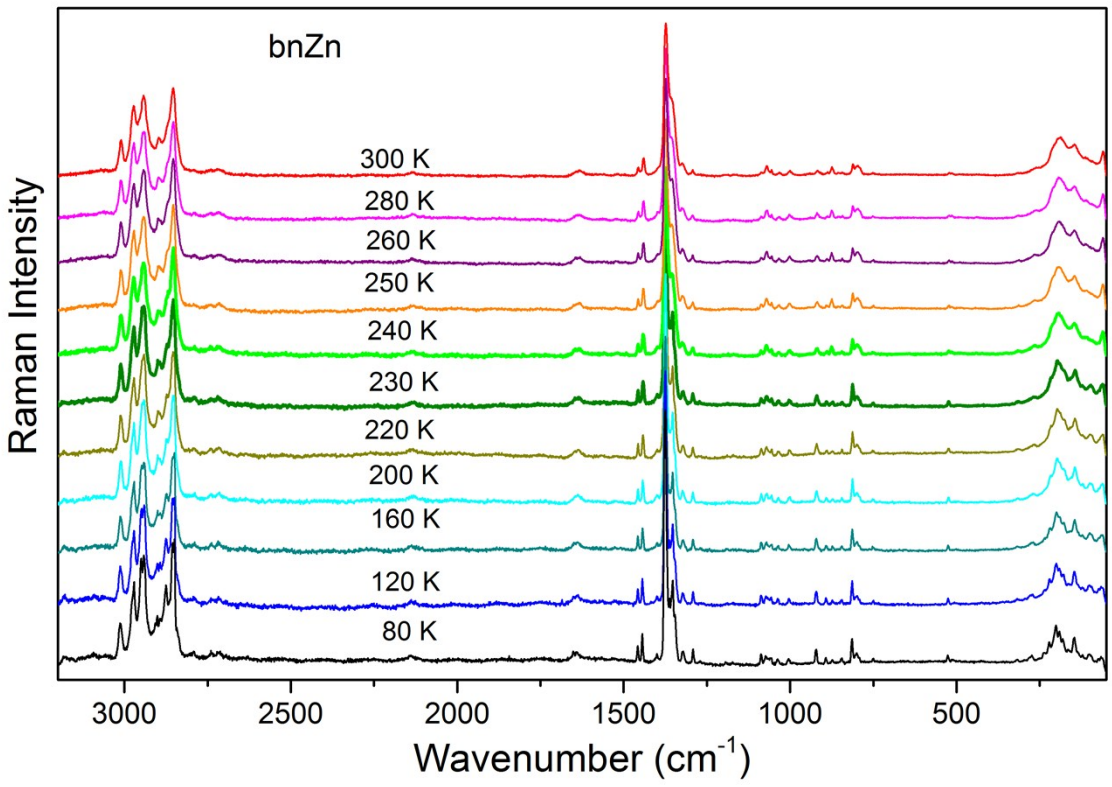

Figure S10. Raman spectra of bnZn recorded at various temperatures.

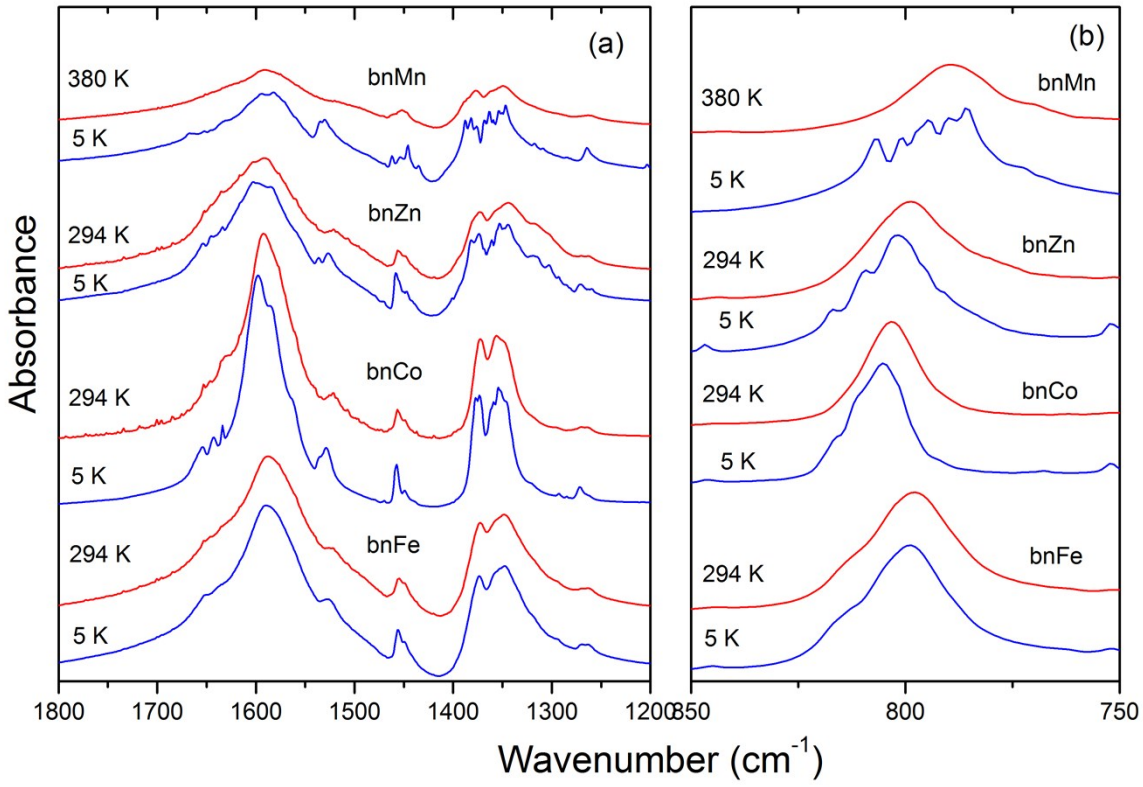

Figure S11. Comparsion of the IR spectra for bnZn, bnCo, bnFe and bnMn in the 1200-1800 and 750-850 cm^{-1} ranges.

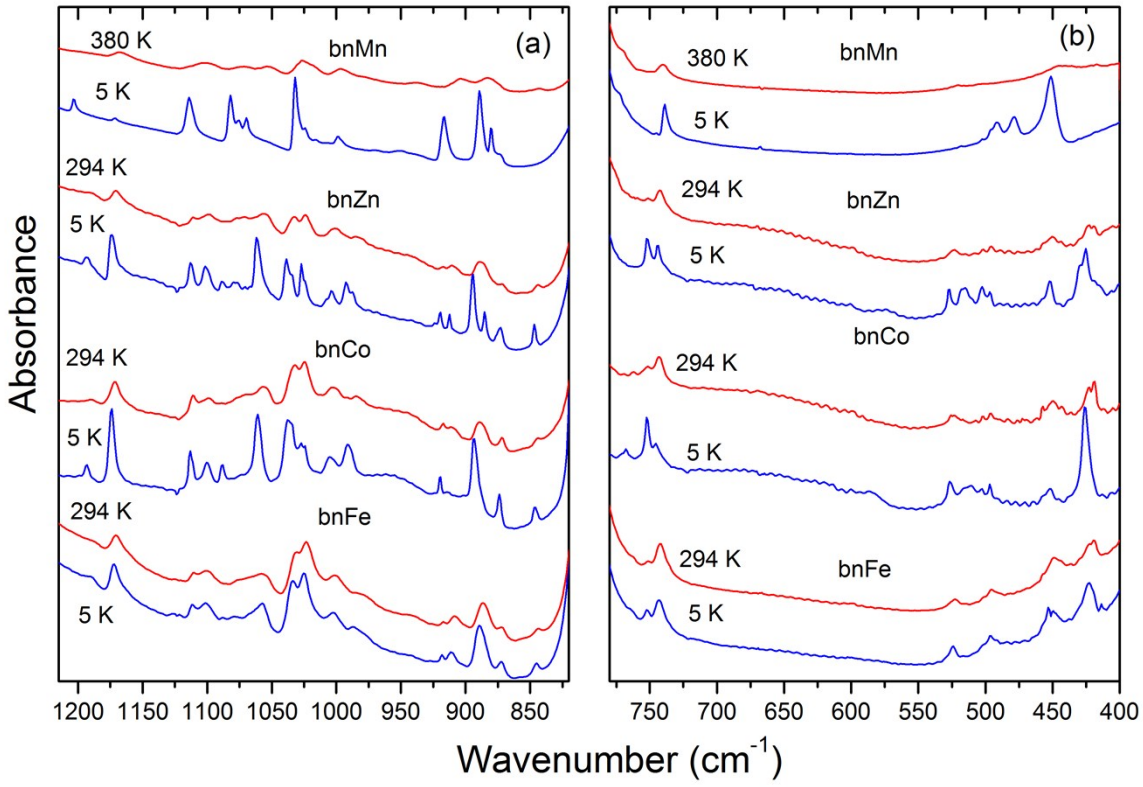

Figure S12. Comparsion of the IR spectra for bnZn, bnCo, bnFe and bnMn in the 820-1215 and 400-780 cm^{-1} ranges.

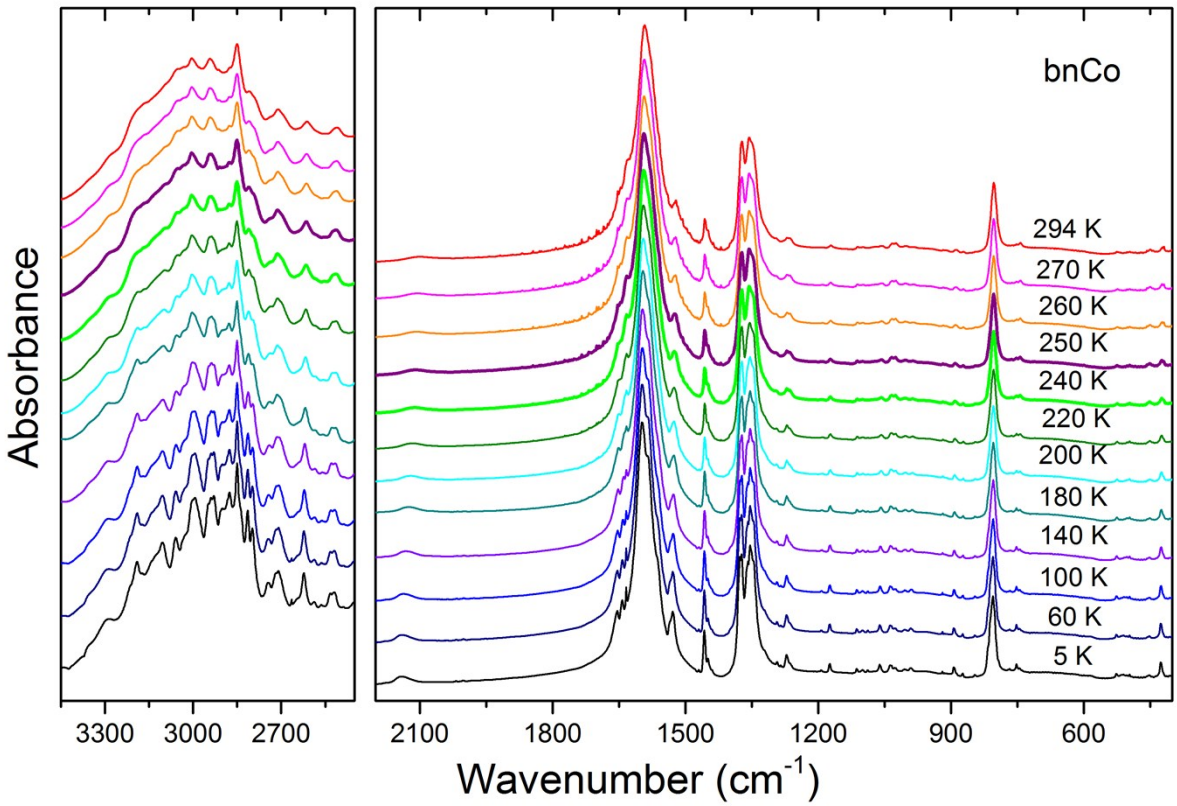

Figure S13. mid-IR spectra of bnCo recorded at various temperatures.

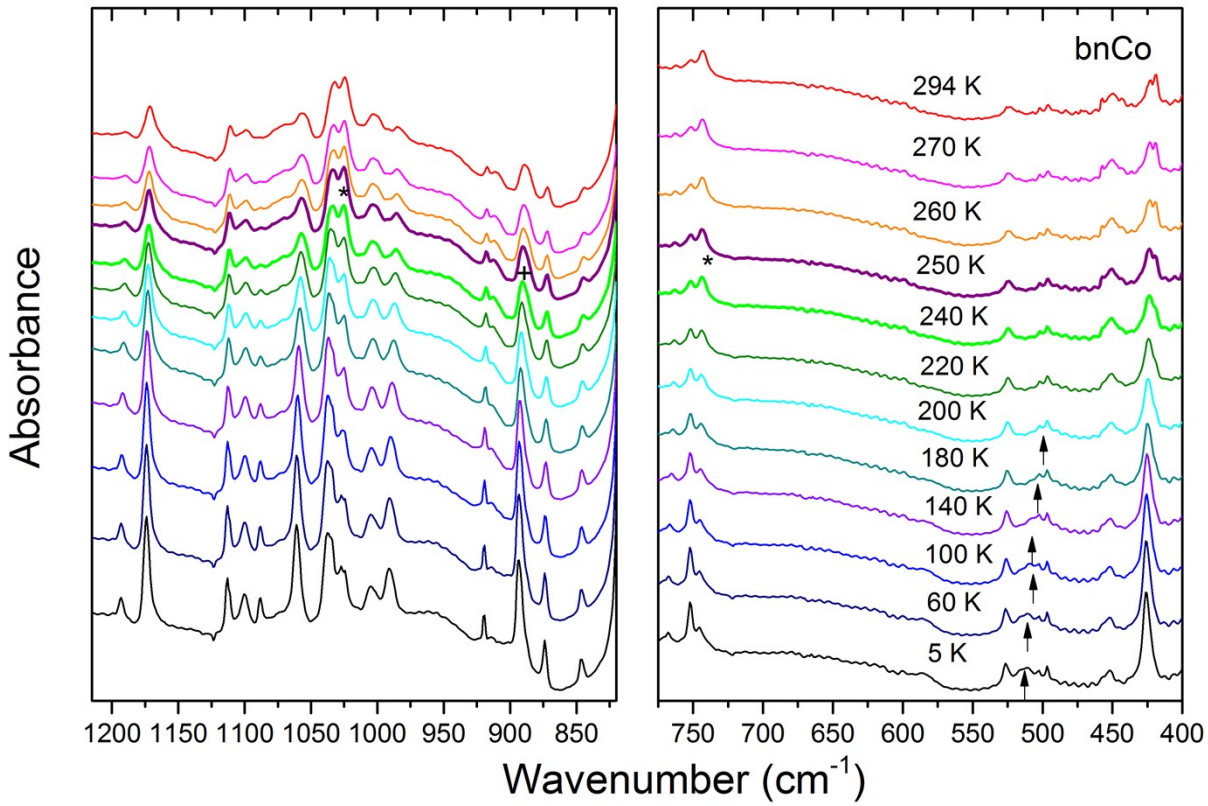

Figure S14. Detail of the IR spectra of bnCo corresponding to the spectral ranges 1215-820 and 775-400 cm^{-1} at different temperatures in cooling run. Asterisks indicate bands that exhibit sudden intensity change near T_C. Cross indicates the band that exhibits most pronounced narrowing upon cooling and arrows show position of a very broad band that exhibits large shift towards higher wavenumbers, narrowing and splitting upon cooling below 240 K.

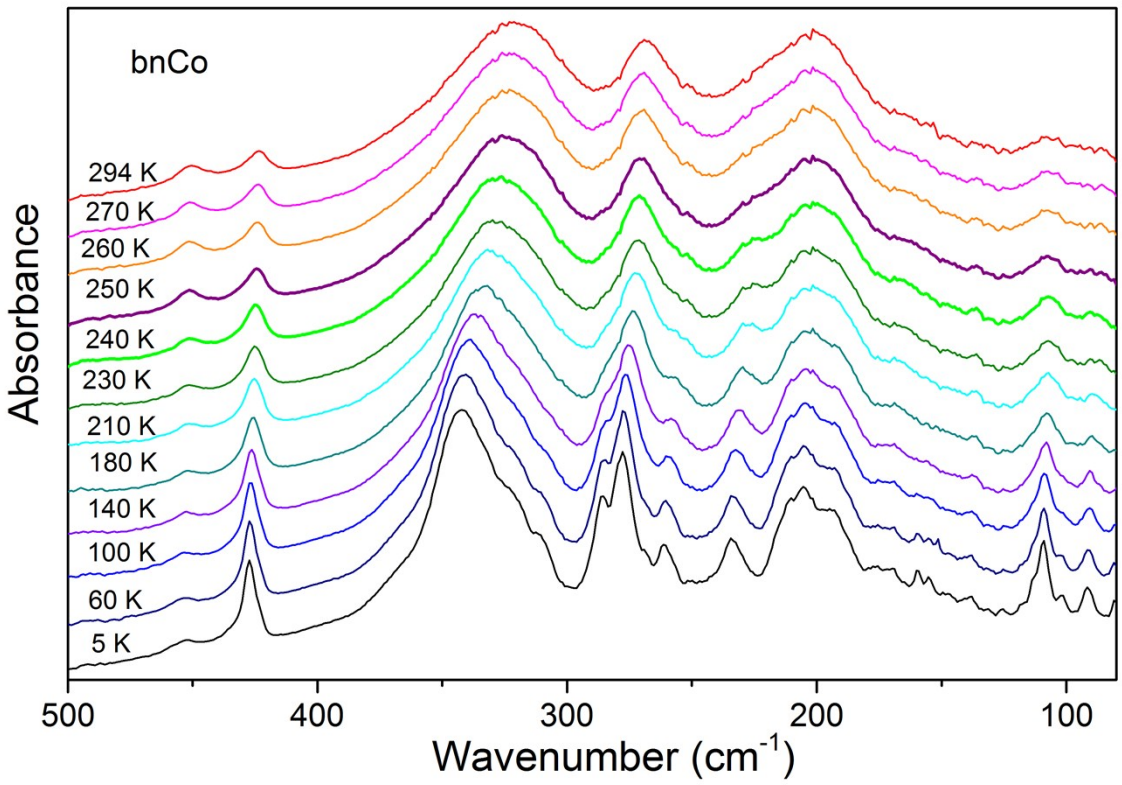

Figure S15. far-IR spectra of bnCo recorded at various temperatures.

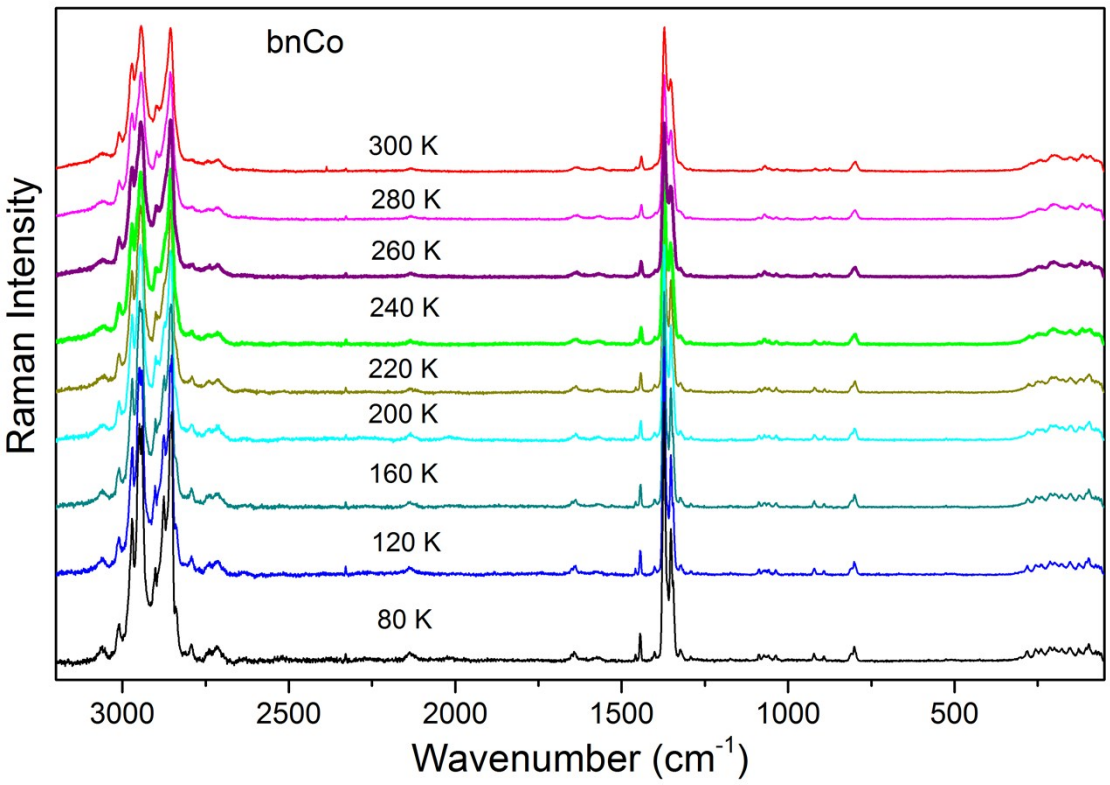

Figure S16. Raman spectra of bnCo recorded at various temperatures.

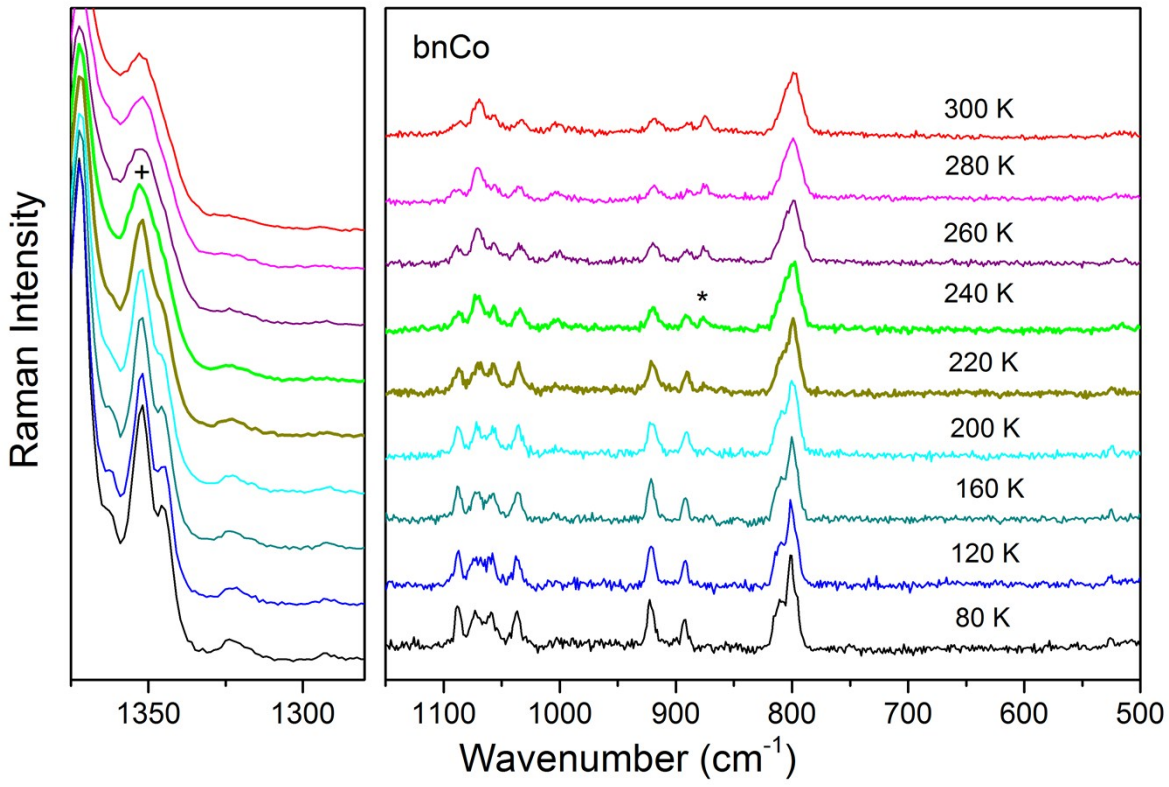

Figure S17. Detail of the Raman spectra of bnCo corresponding to the spectral ranges 1375-1280 and 1150-500 cm^{-1} at different temperatures in heating run. Asterisk indicates band that exhibits sudden intensity change at T_C. Cross indicates the band that exhibits pronounced narrowing near T_C.

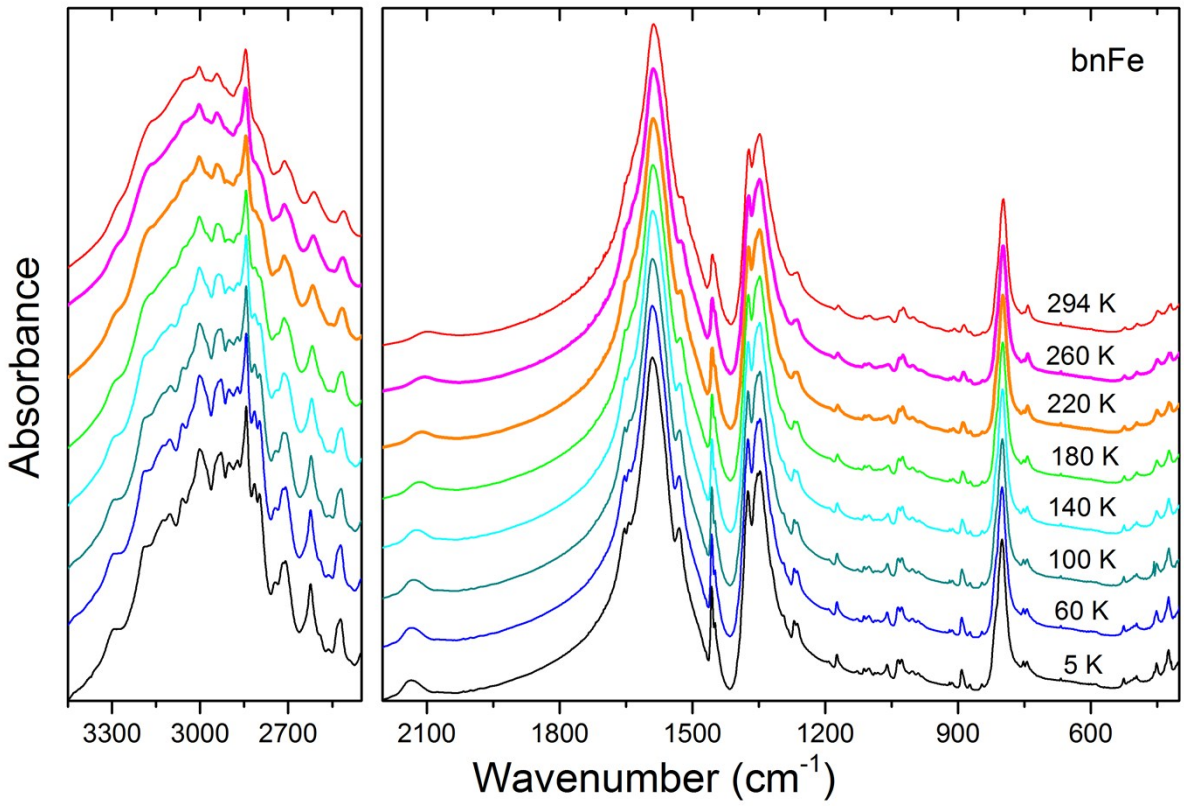

Figure S18. mid-IR spectra of bnFe recorded at various temperatures.

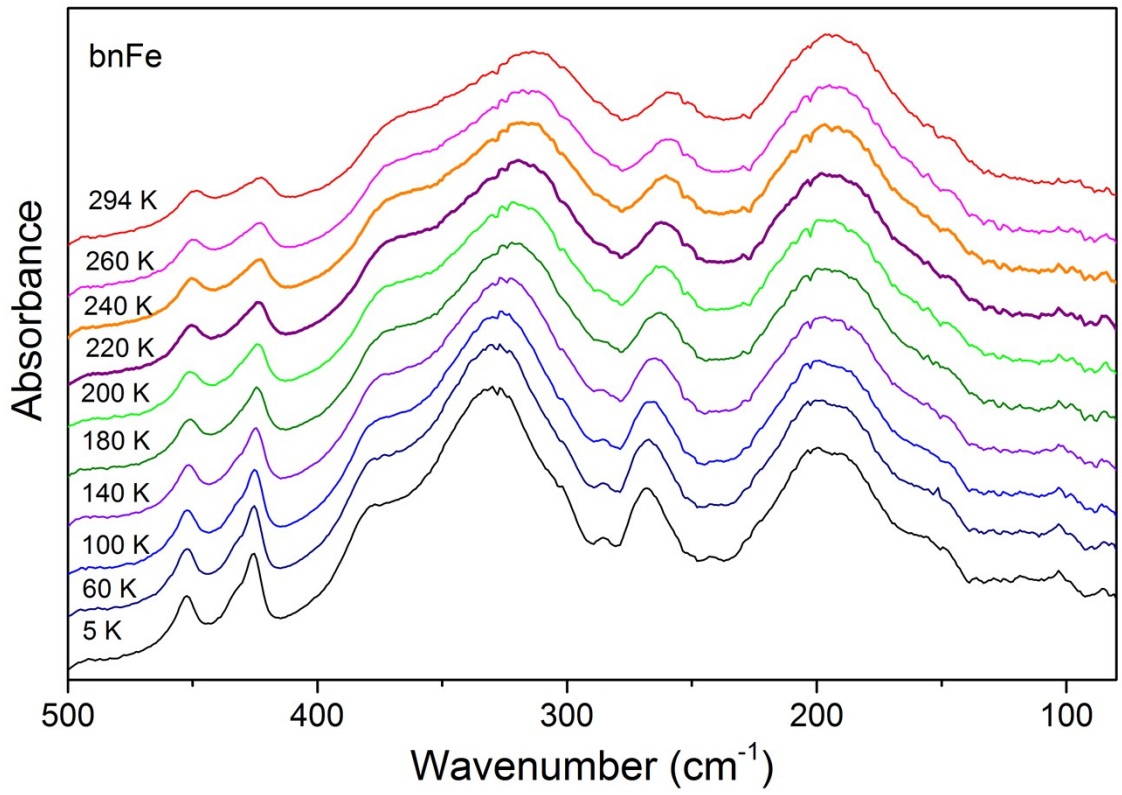

Figure S19. far-IR spectra of bnFe recorded at various temperatures.

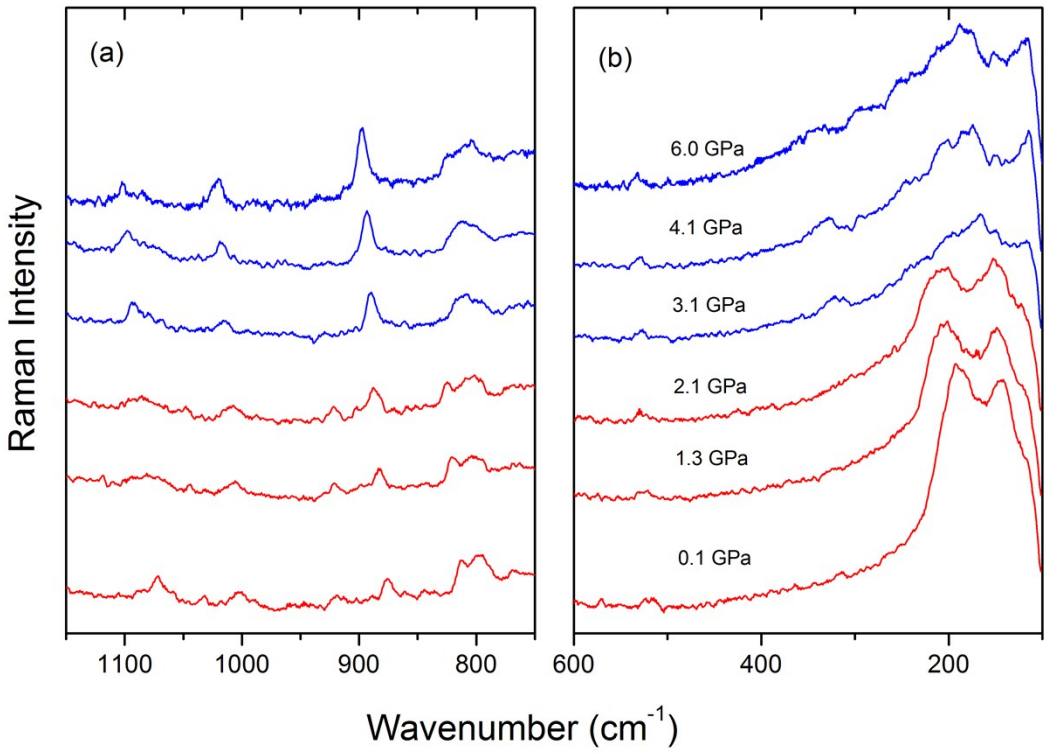

Figure S20. Raman spectra of bnZn recorded during decompression experiment.